Bull. Mater. Sci. (2019) 42:160
https://doi.org/10.1007/s12034-019-1827-z

Mechanical and corrosion performance of multilayer ceramic coatings deposited on an austenitic stainless steel using plasma spray

SEYED RAHIM KIAHOSSEINI* and ARMIN AMINIAN
Department of Engineering, Damghan Branch, Islamic Azad University, Damghan 3671639998, Iran
*Author for correspondence (rkiahoseyni@yahoo.com)

MS received 7 June 2018; accepted 12 December 2018; published online 21 May 2019

Abstract. This research investigated consecutive multilayer thermal barrier coatings, including Ni_3Al–Al_2O_3–Al_2O_3/MgO, produced by plasma spray with outer layer thicknesses of 50, 100 and 150 μm deposited on an AISI 316 stainless steel. X-ray diffraction, scanning electron microscopy, Rockwell-B hardness measurements, pin-on-disk wear test and potentiodynamic polarization test were performed to evaluate the specimens. The results revealed that the structure of the produced coatings was completely crystalline. An increase in the coating thickness formed a smooth surface and a low degree of roughness and promoted grain growth. According to the Hall–Petch equation, the degree of hardness decreased from 99 to 92 HRB, and the friction coefficient decreased from 1.25 to 0.6 because of low surface roughness. An adherence test performed with a Brinell hardness test showed that an increase in the layer thickness improved the coating adherence coefficient (dp/dr) from 0.083 to 0.118 kg μm^{-1}. The corrosion test results indicated that the increase in the coating thickness caused a decrease in corrosion current density from 1.1 to 0.008 mA cm^{-2}.

Keywords. Electrochemical corrosion; wear; polarization; friction coefficient; plasma spray.

1. Introduction

High-temperature austenitic stainless steels are designed for use at <550°C [1,2]. As such, creep is a vital factor influencing fracture formation at this temperature [3–5]. In addition, stainless steels have well resistance to corrosion when they are exposed to dry gases at high temperatures (800–1150°C). They also exhibit high oxidation resistance when they are immersed in a corrosive solution [6–11]. However, hot corrosion with electrochemical corrosion occurs. Nevertheless, thermal barrier coatings should be utilized to improve the lifetime of stainless steels at high temperatures [12–14].

Thermal barrier coatings mainly prevent heat transfer and penetration of corrosive salts in base metal structures. These coatings may be used to increase the efficiency of high-temperature turbines [15–18]. Considering that repairing a turbine to change old blades entails high cost, the development of thermal barrier coatings leads to low-cost repair by depositing a coating instead of replacing old blades. Therefore, the mechanical properties and industrial-scale development of this technology should be evaluated [19–21].

In other studies, the performance of some coatings, such as thermal barriers, has been examined [22–24]. For instance, Huai *et al* [25] characterized the corrosion behaviour of single-layer Al_2O_3 on a steel substrate. They found that by adding Al to the Al_2O_3 coating, the corrosion resistance of the steel increased. Zhou *et al* [26] determined the influence of MgO coating on a low-alloy steel substrate. It was found that the corrosion of the coated sample was reduced by about 65% when compared with uncoated samples. Mishra *et al* [27] analysed the corrosion–wear behaviour of Fe-based super alloys with the help of a Ni_3Al coated layer. Under high temperature conditions, the Ni_3Al coating is oxidized and reduces the erosion–corrosion of the superalloy. However, the performance of composite coatings such as hydroxyapatite/ZrN has yet to be investigated [28,29]. The formation of the coatings in the form of composite layers can create a more uniform stress between the layers and thus, increase in the adhesion of the coatings. In addition, multilayer coatings can also improve the mechanical, electrochemical and optical properties compared to single-layer coatings [28,30].

In our study, Ni_3Al–Al_2O_3–Al_2O_3/MgO composite coatings were deposited on a 316 stainless steel substrate, and their mechanical and electrochemical properties were evaluated. Their properties can indicate the simultaneous effect of three corrosion-wear resistant layers on the characteristics of the coatings.

2. Experimental

Stainless steel disks with a diameter of 3.5 cm and a height of 1 cm were used in this study as a substrate. The surface was prepared with a SiC paper and degreased in ethanol

Table 1. Plasma spraying machine indexes for coating of 316 stainless steel.

Index	Al_2O_3	Ni_3Al	MgO/Al_2O_3
Voltage (V)	50	45	55
Current (A)	600	450	650
Initial gas flow rate (Ar) ($l\,min^{-1}$)	28–30	24–25	55
Secondary gas flow rate (H_2) ($l\,min^{-1}$)	7–9	17	10
Spray distance (mm)	120	110	140
Powder feed ($g\,min^{-1}$)	30	40	25
Thickness of coating (μm)	100	100	50, 100 and 150

(99.9%) and dried by blowing Ar gas. The surfaces of substrates were sand blasted by silica particles with a size of 240 μm under an air pressure of 6 bar and an angle of 90° to optimize the substrate surface roughness and consequently achieve an enhanced bonding between the substrate and the coating. Afterwards, the prepared substrates were coated by Ni_3Al and then, the Al_2O_3 coating was deposited on it. Finally, the outer layer was created with a composition of 60 wt.% Al_2O_3 and 40 wt.% MgO with thicknesses of 50, 100 and 150 μm. The electrodeposition parameters of various coatings produced by the plasma spray method are shown in table 1.

To investigate the microstructure of coatings, an X-ray diffractometer (XRD, model: PANalytical X'Pert Pro MPD), a scanning electron microscope (SEM, model: TeScan—Mira III) and an atomic force microscope (AFM, model: FemtoScan) were used. A Rockwell-B hardness test was conducted to measure the microhardness of multilayer coatings, and a pin-on-disk wear test was carried out according to ASTM G99 standard. For this purpose, a pin with a surface area of 1 mm^2 was used under a load of 0.30 kg on a circular-shaped disk with a speed of 0.10 $m\,s^{-1}$ and a displacement of 100 m. The obtained data were used to plot a diagram of friction coefficient (μ) *vs*. displacement. Mass reduction during the wear test was also calculated.

With a ceramic nature, coatings are stronger than sublayers. As such, the hardness test was performed to evaluate the adherence between coatings. According to the methods described by Kim *et al* [31], a Brinell method was utilized to determine the effects of various parameters on the hardness of the specimens and to draw a plot of the effects of the crack tip size (r) *vs*. the applied force (p). dp/dr was calculated as a factor that indicates the adhesion between the coated layer and the sublayer [32–34].

A potentiodynamic polarization test was used to evaluate the corrosion behaviour of the specimens by an 'EG&G 263A' potentiostat/galvanostat equipped with a saturated calomel reference electrode. The coated samples and the reference sample were submerged in a NaCl solution (3.5%) for 1 h until equilibrium was reached. This test was operated at a potential scanning speed of 1 $mV\,s^{-1}$ in a potential range of −0.25–0.6 V (*vs*. open circuit potential) to plot the results as Tafel diagrams in cathodic and anodic branches.

3. Results and discussion

XRD patterns of the AISI 316 stainless steel coated with different thicknesses of Ni_3Al–Al_2O_3–Al_2O_3/MgO layers are shown in figure 1. With low thickness, X-rays reached the underlying layers, and other irrelevant peaks were observed. When the thickness was increased to 150 μm, only Al_2O_3 and MgO peaks were visible.

SEM images of the surface of the samples coated with Ni_3Al–Al_2O_3–Al_2O_3/MgO are presented in figure 2. An increase in the coating time resulted in homogenized and contiguous particles. With the further extension of the spraying time, numerous particles were deposited on the surface, and the temperature and time were sufficient for grain growth. In figure 2c, some cracks were observed on the coating surface when the thickness of the coating increased. These cracks could be a result of internal stress due to grain growth and grain strike.

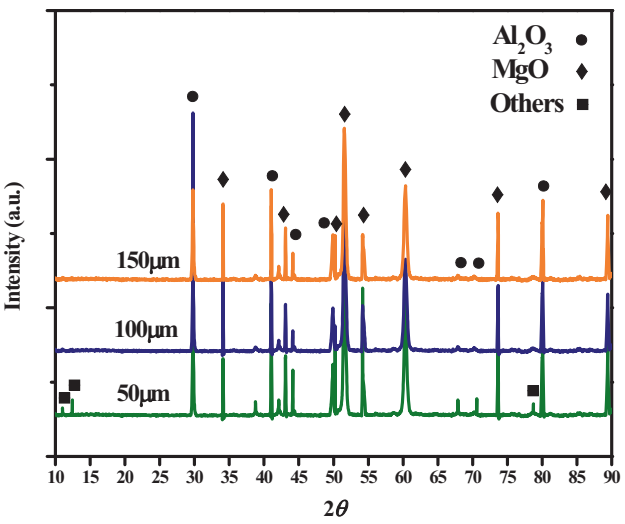

Figure 1. XRD patterns of the AISI 316 stainless steel coated with different thicknesses of Ni_3Al–Al_2O_3–MgO/Al_2O_3 layers with various thicknesses of the Al_2O_3/MgO outer layer.

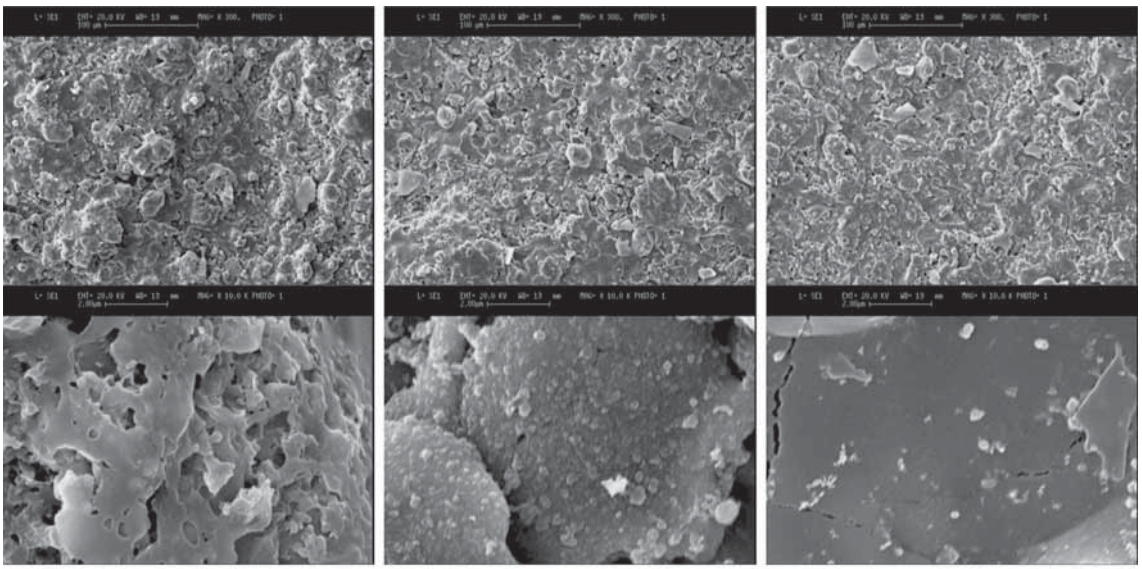

Figure 2. SEM images of the AISI 316 stainless steel coated with Ni_3Al–Al_2O_3–MgO/Al_2O_3 layers with various thicknesses of the Al_2O_3/MgO outer layer: (**a**) 50, (**b**) 100 and (**c**) 150 μm with magnification of 300× and 10,000×.

Hardness measurement results of the samples coated with various thicknesses of Ni_3Al–Al_2O_3–Al_2O_3/MgO layers are presented in figure 3. The coating thickness increased, and the degree of hardness decreased. The samples were different because the deposition time applied to them varied. Heat transfer in thick layers is longer than that in thin layers according to equation (1) [35] because of the high melting point of such materials. Consequently, grains have enough time to grow.

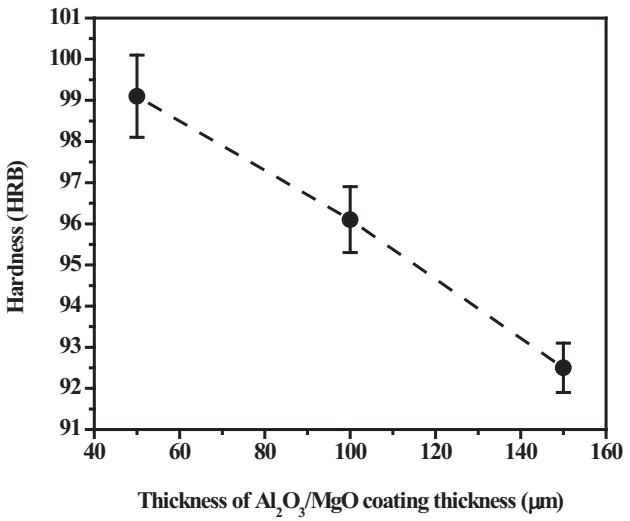

Figure 3. Hardness measurement results of the AISI 316 stainless steel coated with different thicknesses of Ni_3Al–Al_2O_3–MgO/Al_2O_3 layers with various thicknesses of the Al_2O_3/MgO outer layer. The bars show mean ($n = 5$) ± SD. Different letters on the bars represent the significance difference at 5% probability level.

$$d^2 - d_0^2 = kt, \tag{1}$$

where d is the grain size during heat treatment, d_0 is the primary grain size, k is the factor dependent on temperature and t is the time when temperature increases. Therefore, increasing the time to achieve high temperatures is suitable for grain growth. According to the Hall–Petch equation [36,37] (equation (2)), an increase in the grain size results in a low degree of hardness. For this equation, σ_0 is the yield stress, K_s is the constant dependent on material nature and d is the grain size.

$$\sigma_y = \sigma_0 + \frac{k_s}{\sqrt{d}}. \tag{2}$$

The results of the friction coefficient analysis of the coated samples are illustrated in figure 4a. The highest friction coefficient corresponded to the sample with an outer layer thickness of 50 μm. In figure 5, the AFM results revealed that the sample was more non-uniform and lumpy than the other samples that could affect the friction coefficient. For a wear distance of 35 m, spontaneity of the friction coefficient decreased from 1.5 to 1 likely because of complete coating deterioration due to low thickness and pin movement along the outer layer, Al_2O_3/MgO, and the middle Al_2O_3 layer. The friction coefficient increased because of the worn particles, thereby reaching a constant rate. Increasing the thickness and uniformity of the surface caused the horizontal force to decrease, and the friction coefficient finally decreased.

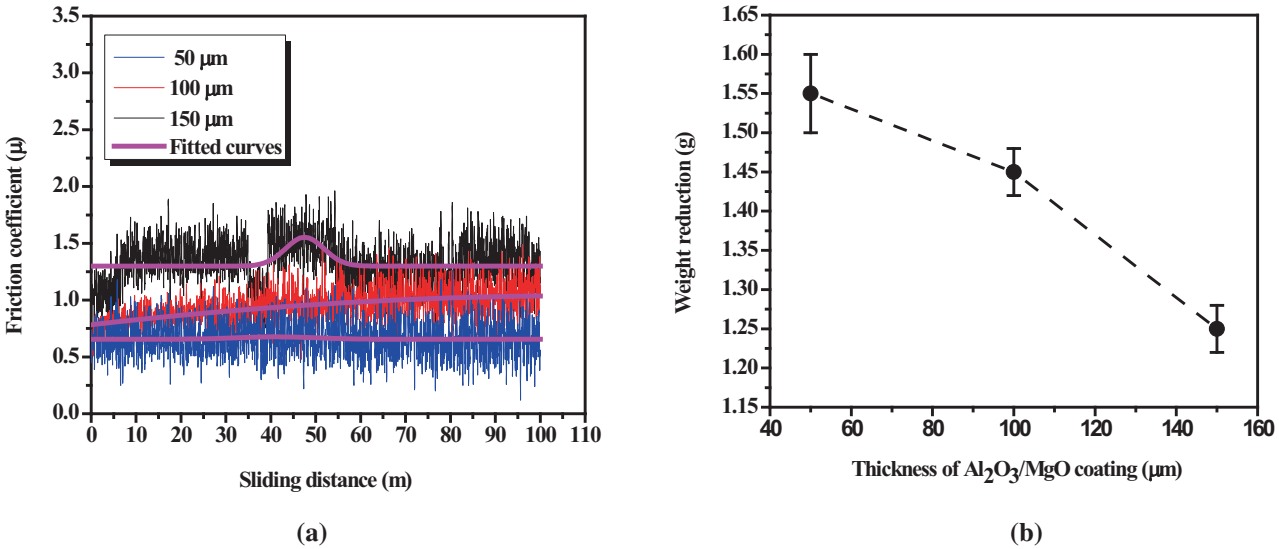

Figure 4. (**a**) Wear test (pin-on-disk) results. (**b**) Mass reduction of the AISI 316 stainless steel coated with Ni_3Al–Al_2O_3–MgO/Al_2O_3 layers with various thicknesses of the Al_2O_3/MgO outer layer. The bars show mean ($n = 5$) ± SD. Different letters on the bars represent the significant difference at 5% probability level.

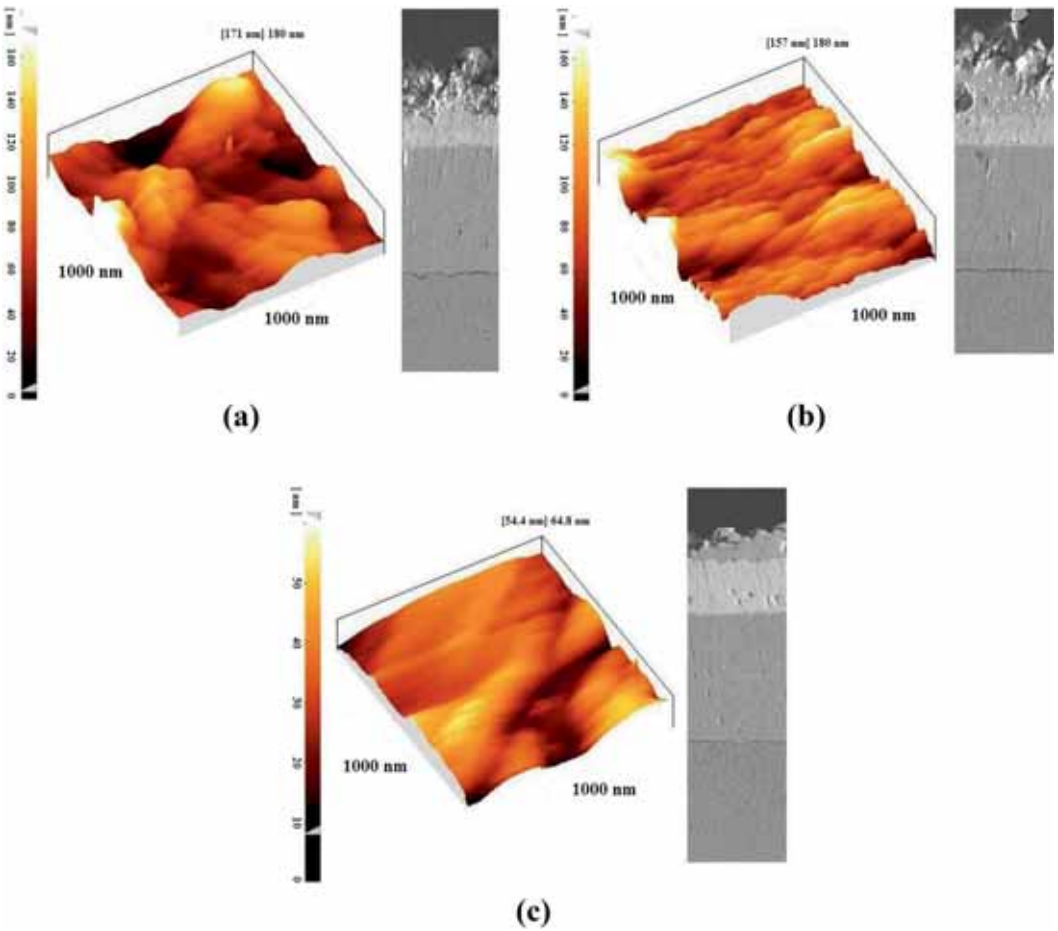

Figure 5. AFM results and SEM cross-section images of the AISI 316 stainless steel coated with Ni_3Al–Al_2O_3–MgO/Al_2O_3 layers with various thicknesses of the Al_2O_3/MgO outer layer: (**a**) 50, (**b**) 100 and (**c**) 150 µm.

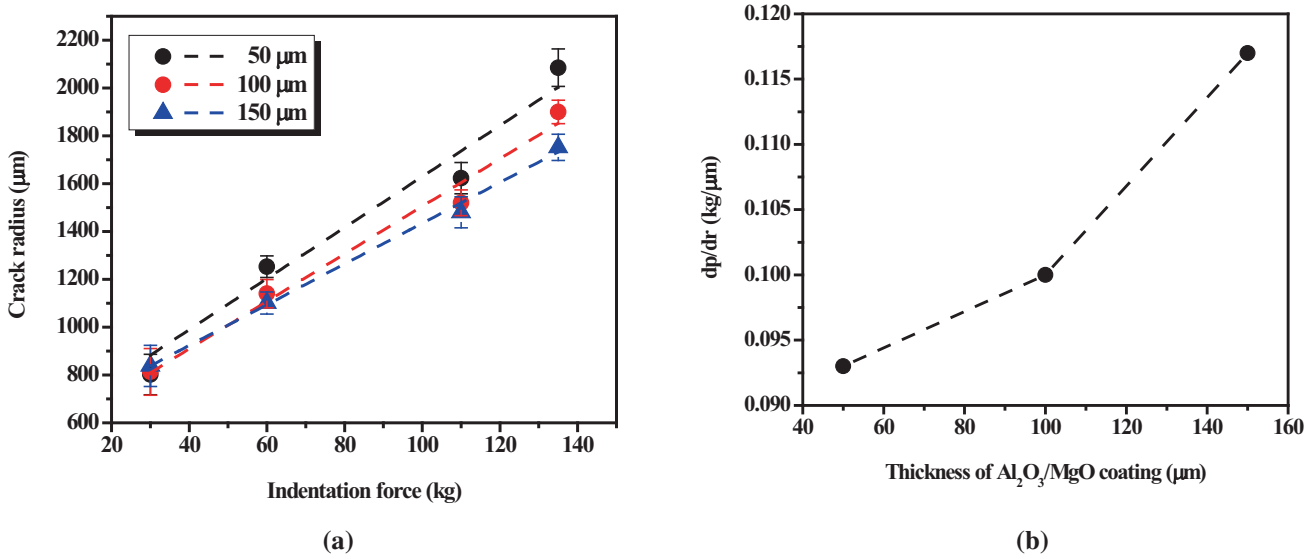

Figure 6. (**a**) Radius of the cracks due to the indenter effect on the sampling area *vs*. the increasing penetration force. (**b**) Variation in dp/dr *vs* the thickness of the AISI 316 stainless steel coated with different thicknesses of Ni_3Al–Al_2O_3–MgO/Al_2O_3 layers.

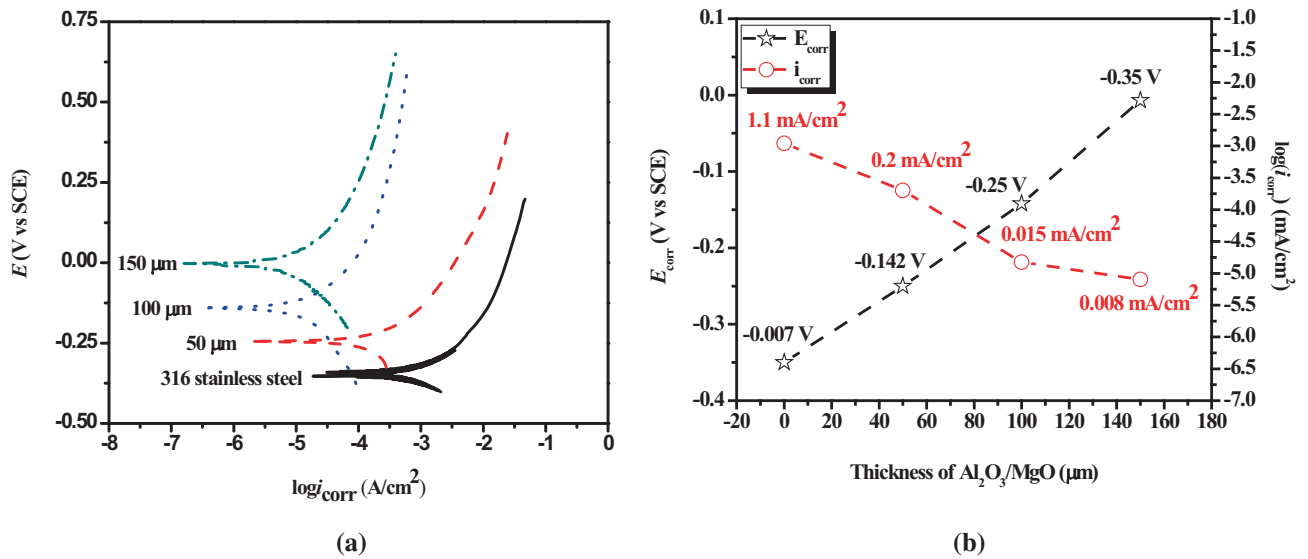

Figure 7. (**a**) Potentiodynamic polarization diagram. (**b**) Tafel analysis from the polarization diagrams for the 316 stainless steel in a NaCl solution (3.5%) before and after the steel was coated with different thicknesses of Ni_3Al–Al_2O_3–MgO/Al_2O_3 layers (50, 100 and 150 µm).

The mass reduction of the samples after the wear test is presented in figure 4b. With an increase in the coating thickness and a decrease in the surface roughness, the degree of mass reduction decreased, indicating a low degree of abrasion. Therefore, a low friction coefficient corresponded to low mass reduction.

The results of the adhesion test of the AISI 316 stainless steel coated with different thicknesses of $MgNi_3Al$–Al_2O_3–Al_2O_3/MgO layers are shown in figure 6. For this test, dp/dr was considered as the adhesion factor. Thick layers needed an extended time, thereby relieving the stress on sublayers. For thin samples, adhesion was low because of fast solidification that induced high stress. The internal stress created in the coating with a thickening that was so high when coated with a thickness of >150 µm, the coating was cracked and did not have the proper adhesion.

Figure 7 shows the results of the potentiodynamic polarization test of the AISI 316 stainless steel coated with different thicknesses of Ni_3Al–Al_2O_3–Al_2O_3/MgO layers before and after coating. All the samples exhibited an active behaviour and a passive behaviour was not observed in the anodic branch. As such, the corrosion products could not protect

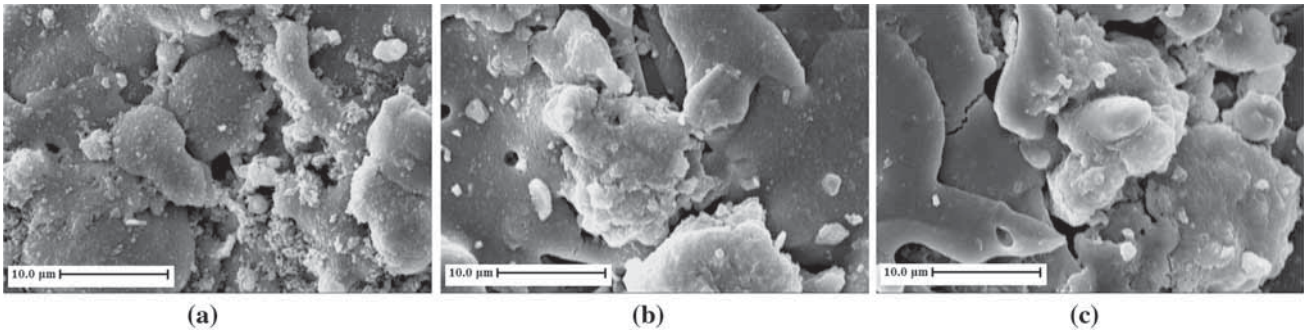

Figure 8. SEM images of the corroded surface of the AISI 316 stainless steel coated with different thicknesses of Ni_3Al–Al_2O_3–MgO/Al_2O_3 layers with various thicknesses of the Al_2O_3/MgO outer layer: (**a**) 5, (**b**) 10 and (**c**) 15 μm.

the sample surfaces. By increasing the thickness of the coating, the polarization results (cathodic and anodic polarization plots) approach the more positive potentials, so that the corrosion potential increases from −0.35 to 0 V *vs*. saturated calomel electrode. As a result, with increasing the thickness of the coating, the tendency of the sample to corrosion is reduced. Among the samples, the stainless steel sample without a coated layer showed the highest corrosion current and more negative potentials, indicating low corrosion resistance (figure 7b). Thus, the deposition of the Ni_3Al–Al_2O_3–Al_2O_3/MgO surface composite affected the corrosion resistance of the AISI 316 stainless steel. The thickness of Al_2O_3/MgO increased, and the corrosion current decreased significantly from 1.1 (without coating) to 0.008 mA cm^{-2} for the Ni_3Al–Al_2O_3–Al_2O_3/MgO sample with a thickness of 150 μm. In figure 5, an increase in the coating thickness resulted in the formation of a uniform layer due to numerous deposits on the surface. Hence, the attracted Cl^- hardly penetrated the coating, and corrosion resistance increased. An increase in the thickness also strengthened the adhesion between the layer and the sublayer, thereby significantly affecting the corrosion resistance.

The corroded sample surfaces were evaluated through SEM (figure 8). The coated sample with a thickness of 50 μm was completely corroded because its fine structure and numerous grain boundaries favoured corrosion. Intergranular corrosion occurred, and grains were clearly distinguished. For the coated sample with a thickness of 150 μm, favourable paths for attack were produced through crack formation, although few grain boundaries existed. The corrosion current density eventually decreased.

4. Conclusion

AISI 316 stainless steels were coated with Ni_3Al–Al_2O_3–Al_2O_3/MgO layers with various thicknesses of Al_2O_3/MgO outer layer. The following results are obtained:

The coated layers had a crystal structure. As the outer layer thickness increased, the degree of hardness decreased because of grain growth on coating. With a low degree of surface roughness, the friction coefficient decreased and wear resistance improved. For the thick samples, the time to relieve stress on the coating was sufficient. Consequently, the adhesion between layers increased. The corrosion resistance of the thick samples was also high because of the high degree of adhesion between layers and the considerable uniformity of the coating.

References

[1] Pommier H, Busso E, Morgeneyer T and Pineau A 2017 *Eng. Fract. Mech.* **183** 170
[2] Gross C T, Jiang Z, Mathai A and Chung Y-W 2016 *Surf. Sci.* **648** 196
[3] Nikulin I, Kaibyshev R and Skorobogatykh V 2010 *J. Phys. Conf. Ser.* **240** 012071
[4] Margolin B, Gulenko A and Buchatsky A 2009 *ASME 2009 pressure vessels and piping conference* p 949
[5] Ghazani M S, Eghbali B and Ebrahimi G R 2017 *Trans. Indian Inst. Metals* **70** 1755
[6] Brady M P, Magee J, Yamamoto Y, Helmick D and Wang L 2014 *Mater. Sci. Eng. A* **590** 101
[7] Firouzdor V, Sridharan K, Cao G, Anderson M and Allen T 2013 *Corros. Sci.* **69** 281
[8] Gupta R and Birbilis N 2015 *Corros. Sci.* **92** 1
[9] Chinizadeh M and Kiahosseini S R 2017 *J. Mater. Res.* **32** 1
[10] Pitkänen H, Alatalo M, Puisto A, Ropo M, Kokko K and Vitos L 2013 *Surf. Sci.* **609** 190
[11] Sharma N K and Shekhar S 2017 *Trans. Indian Inst. Metals* **70** 1277
[12] Pereira J, Zambrano J, Tobar M, Yañez A and Amigó V 2015 *Surf. Coat. Technol.* **270** 243
[13] Lazar A-M, Yespica W P, Marcelin S, Pébère N, Samélor D, Tendero C *et al* 2014 *Corros. Sci.* **81** 125
[14] Shirazi A K and Kiahosseini S R 2017 *Int. J. Mater. Res.* **108** 675
[15] Aydin H 2013 *Appl. Therm. Eng.* **51** 623
[16] O'Donnell R, Powell T, Hoffman M, Jordan E and Filipi Z 2017 *J. Eng. Gas Turb. Power* **139** 102808
[17] Tang Q, Liu J, Dai J and Yu Z 2017 *Appl. Therm. Eng.* **114** 770
[18] Avci A, Eker A A and Eker B 2018 in *Microstructure and oxidation behavior of atmospheric plasma-sprayed thermal barrier coatings* I Dincer, C Ozgur Colpan and O Kizilkan (eds) (San Diego, United states: Elsevier Science Publishing Co Inc) p 793

[19] Darolia R 2013 *Int. Mater. Rev.* **58** 315
[20] Huda Z and Edi P 2013 *Mater. Des.* **46** 552
[21] Mauer G, Jarligo M O, Mack D E and Vaßen R 2013 *J. Therm. Spray Technol.* **22** 646
[22] Häber T and Suntz R 2018 *Int. J. Heat Fluid Flow* **69** 95
[23] Yu J, Wang Y, Zhou F, Wang L and Pan Z 2018 *Appl. Surf. Sci.* **431** 112
[24] Sachidananda K, Mahesha K and Dey A 2018 *Ceram. Int.* **44** 158
[25] Huai X, Zhao S and Li W 2009 *J. Ceram. Process. Res.* **10** 618
[26] Zhou X, Ye S, Xu H, Liu P, Wang X and Wei L 2012 *Surf. Coat. Technol.* **206** 3619
[27] Mishra S, Chandra K and Prakash S 2017 *Anti-Corros. Methods Mater.* **64** 540
[28] Kiahosseini S R, Afshar A, Larijani M M and Yousefpour M 2017 *Appl. Surf. Sci.* **401** 172
[29] Kiahosseini S R, Afshar A, Larijani M M and Yousefpour M 2015 *J. Chem. Health Risks* **5** 45
[30] Majidi H, Aliofkhazraei M, Karimzadeh A and Rouhaghdam A S 2016 *Bull. Mater. Sci.* **39** 1691
[31] Kim J-J, Jeong J-H, Lee K-R and Kwon D 2003 *Thin Solid Films* **441** 172
[32] Kiahosseini S R, Afshar A, Larijani M M and Yousefpour M 2013 *J. Mater. Res.* **28** 2709
[33] Fooladi S and Kiahosseini S R 2017 *J. Mater. Res.* **32** 1
[34] Kiahosseini S R and Larijani M M 2017 *Appl. Phys. A* **123** 759
[35] Chen D, Jordan E J, Gell M and Ma X 2009 A C Society (ed) *Dens alumina–zirconia coatings using the solution precursor plasma spray process* (USA: Wiley & Sons) p 223
[36] Langer J 2017 *Phys. Rev. E* **95** 033004
[37] Kiahosseini S R, Baygi S J M, Khalaj G, Khoshakhlagh A and Samadipour R 2018 *J. Mater. Eng. Perform.* **27** 271